

KIC 5197256: an eclipsing binary containing a δ Scuti variable star

Cheng-Long Lv (吕成龙)^{1,2}, Ali Esamdin (艾力·伊沙木丁)^{1,2}, Jun-Hui Liu (刘军辉)³,
Xiang-Yun Zeng (曾祥云)^{1,2} and Tao-Zhi Yang (杨涛只)⁴

¹ Xinjiang Astronomical Observatory, Chinese Academy of Sciences, Urumqi 830011, China; aliyi@xao.ac.cn

² University of Chinese Academy of Sciences, Beijing 100049, China

³ Department of Astronomy, Xiamen University, Xiamen 361005, China; liujunhui@stu.xmu.edu.cn

⁴ School of Physics, Xi'an Jiaotong University, Xi'an 710049, China

Received 2021 March 10; accepted 2021 May 3

Abstract This paper reports analysis of an eclipsing binary system KIC 5197256 with a δ Sct variable component. Utilizing light-curve modeling, several stellar parameters are derived, e.g., temperature, mass, and mass ratio. The $O - C$ diagram is a straight line with a negative slope which means that its period is almost constant for about 2 yr. Frequency analyses are performed for the residual light curve after subtracting the binary variations. The frequency spectrum reveals that one component star is a δ Scuti variable. Large frequency separation is cross-identified with the histogram graph and the Fourier transform method. Based on the large separation and density relationship, the mean density of the δ Sct component is estimated to be $0.05 \text{ g}\cdot\text{cm}^{-3}$. Five frequencies with the same frequency spacing in the range of $25 \text{ d}^{-1} - 34 \text{ d}^{-1}$ are detected. Statistically, the pulsation amplitudes of δ Sct stars increase with decreasing of rotations, so we propose that KIC 5197256 might have a relatively large rotational velocity, and the frequency f_{10} might be the rotation frequency.

Key words: binaries: eclipsing-stars: individual: KIC 5197256— stars: variables: δ Scuti — stars: oscillations

1 INTRODUCTION

The primary goal of the *Kepler* mission is to discover earth-like planets in the habitable zone using transit methods (Koch et al. 2010). The spacecraft was launched into an earth orbit of 372.5 d in March 2009. The high duty-cycle (Koch et al. 2010) and 1470.5 d (4 yr) of data make it possible to probe the structure of stars more precisely than any ground-based telescopes. Two modes of observations were used, i.e., 29.5 min long cadence (LC) and 58.5 s short cadence (SC), respectively (Gilliland et al. 2010). So far, more than 2878 eclipsing binary stars (Kirk et al. 2016) have been detected by the *Kepler* telescope (Borucki et al. 2010; Koch et al. 2010) and at least 2000 δ Sct stars have also been detected in their main fields of view (Balona & Dziembowski 2011; Balona 2014; Bowman et al. 2016). Eclipsing binaries (EBs) are often considered to be our main source of precise access to fundamental stellar parameters, such as the mass and radius of each component. These appropriate parameters can advance our comprehension of stellar models and evolution (Torres et al. 2010). The time of mid-eclipse can also be determined by high-precision and long-term

photometric time series. These time measurements allow the discovery of additional components and/or the study of various physical phenomena that lead to the variation of the EBs orbital period (Hilditch 2001; Kreiner et al. 2001).

Among the pulsating EBs, more than 90 systems are considered to be δ Sct type EBs, while they are also known as oscillating eclipsing Algol (oEA) stars (Mkrtychian et al. 2004; Liakos & Niarchos 2017). The δ Sct stars are short-period pulsators with spectral types ranging from A to F and located in the lower part of the classical Cepheid instability strip. The typical pulsation periods are in the range of 0.02–0.25 d and the amplitudes are generally less than 0.1 mag (Breger 2000; Rodríguez & Breger 2001). In general, δ Sct pulsates in low-order radial/non-radial pressure (p) modes, driven by the κ mechanism of He II partial ionization. It is possible to use these modes to probe the stellar envelope. Pulsations of δ Sct variable stars in binaries have some similar characteristics to those of single δ Sct stars, however, the former pulsations may be a function of mass transfer and companion gravity between the two components. Liakos & Niarchos (2015, 2016) found a threshold for an orbital

Table 1 KIC 5197256 Observational (Photometry) Data Characteristics

Parameters	Values in Catalog	
Kepler ID	5197256	
2MASS ID	19383382+4019257	
Gaia ID	2076547315306055040	
RA, Dec	+19 ^h :38 ^m :33.8 ^s , +40 ^o :19′:25.9″	
BJD ₀	2454953.5389	
Rayleigh f_{res}	0.00508	d ⁻¹
Period	6.96346	d
Kmag	11.024	
T_{eff}	7609	K
$\log g$	3.879	cgs
$\frac{R}{R_{\odot}}$	2.321	
$\frac{F_e}{H}$	-0.22	cgs

These parameters are from the KASOC: <https://kasoc.phys.au.dk/>.

period of about 13 d. When the orbital period is below this threshold, the pulsation of the star is affected by the binarity. Furthermore, in eccentric orbiting binaries, some pulsations could be excited by tidal interactions, resulting excitation modes at frequencies that are multiples of the orbital frequency (Welsh et al. 2011; Hambleton et al. 2013). Liakos et al. (2012), Kahraman Aliçavuş et al. (2017) and Liakos & Niarchos (2017) revealed that the pulsation frequencies are correlated with basic stellar characteristics. Moreover, based on observations of these systems, a scaling relation between the mean stellar density and the pulsation frequency is derived by García Hernández et al. (2015). However, the sample of the eclipsing binary with a δ Sct component is still insufficient, and more eclipsing δ Sct stars need to be investigated in detail.

In this paper, we present a study of KIC 5197256 (RA = 19:38:33.8, Dec = 40:19:25.9 J2000). The basic parameters of KIC 5197256 collected from the Kepler Input Catalog (KIC; Brown et al. 2011). The star is found to be an eclipsing binary with a δ Sct variable component or ellipsoidal variable star (Uytterhoeven et al. 2011; Turner & Holaday 2015; Murphy et al. 2018). Here we report the detailed eclipse and frequency study of KIC 5197256. Section 2 is the observations and data reduction. We model the light curve and apply the classical $O - C$ analysis to KIC 5197256 in Section 3 while analyzing the stellar pulsation in Section 4. The discussion is presented in Section 5. Finally, we make conclusions in Section 6.

2 OBSERVATIONS

From BJD 2455246.29 to 2455275.21 (Q4.3: 42 450 SC observations), KIC 5197256 was observed continuously over 29 d, from BJD 2454953.53 to 2456424.00 (Q0 – Q17: 23 104 LC observations) spanning about 612 d. The SC and LC photometric time series data for KIC 5197256 are all available by the Kepler Asteroseismic

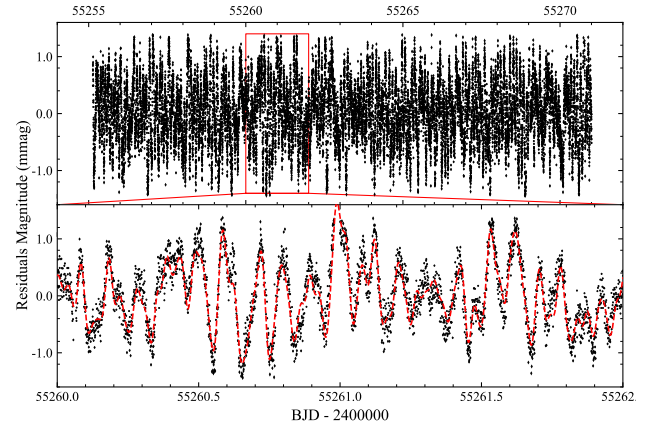


Fig. 1 Residuals of the observed light curve after subtracting of the binarity effects. A partial graph in the bottom panel of the residuals represents the *red inset box* marked in the top panel. The *red dashed line* represents the synthetic curve which is computed using Fourier series fitting with 34-frequencies.

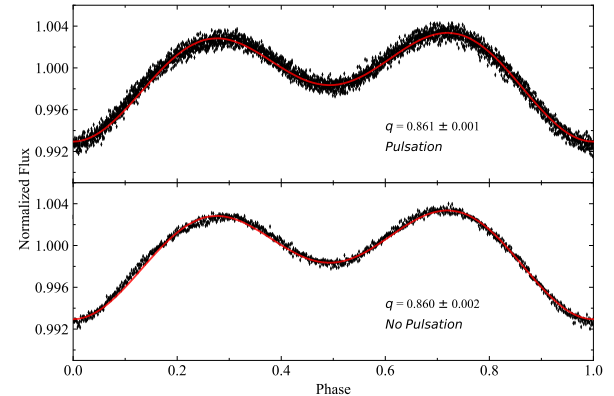


Fig. 2 The binary light curves before (*top*) and after (*bottom*) removal of the pulsation signal from the observed Kepler data are compared. The *red solid curve* is the theoretical light curve, calculated from the W-D code, and the pulsation and no-pulsation parameters ($q \sim 0.861$) are shown in Table 2, respectively.

Science Operations Center (KASOC) data base⁴ (Kjeldsen et al. 2010) with two types: fluxes labeled as “raw” that have been reduced by the NASA Kepler science pipeline, and corrected fluxes made by KASOC Working Group 4 (WG # 4: δ Sct targets). The corrected fluxes have been corrected for cooling down, cooling up, outliers, and jumps. We used the corrected fluxes and converted them to magnitudes, then subtracted the average value of each quarter to obtain the corrected time series. Figure 1 shows the light residuals of KIC 5197256 in SC data, after removal of binary effects (the detailed binary modeling is presented in Sect. 3.1). The pulsation features can be seen clearly in the bottom panel of Figure 1.

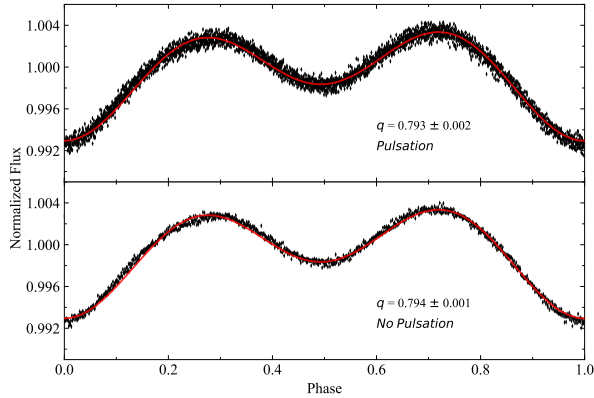


Fig. 3 The binary light curves before (*top*) and after (*bottom*) removal of the pulsation signal from the observed Kepler data are compared. The *red solid curve* is the theoretical light curve, calculated from the W-D code, and the pulsation and no-pulsation parameters ($q \sim 0.793$) are shown in Table 3, respectively.

3 ECLIPSING

3.1 Binary Modeling

The 2013 version of the Wilson-Devinney (W-D) code (Wilson & Devinney 1971; Wilson 1979, 2012) is utilised to fit the light curve of KIC 5197256 in the *Kepler* band. In the fitting process, the hotter component is defined as a primary star with subscript 1 and the cooler one is a secondary star with subscript 2. The initial effective temperature T_1 of the primary star is set as 7830K based on the spectral type A7V collected from LAMOST DR7 (Cui et al. 2012). A circular orbit and synchronous rotation are assumed. For the bolometric limb darkening law, we utilize the logarithmic form with the coefficients, X_{bolo} and Y_{bolo} , taken from van Hamme (1993) while the gravity darkening coefficients and the bolometric albedos are set to $g_1 = g_2 = 1.0$ (Lucy 1967) and $A_1 = A_2 = 1.0$ (Ruciński 1969). The adjustable parameters are the orbit inclination i , the mean surface temperature of secondary T_2 , the modified dimensionless surface potential Ω_1 , and the band-pass luminosity of primary L_1 .

The mass ratio q , representing the mass of primary M_1 over that of secondary M_2 , is a crucial parameter in the light-curve analysis. However, there is no appropriate value based on spectroscopic radiative velocity curves or photometric solutions yet. Thus, a current method called the q-search procedure is used to obtain an initial value of q . In this procedure, the value of the mass ratio is set to vary from 0.1 to 1.0 in a step of 0.01 and fixed at each time light-curve fitting. As shown in Figure 4, we obtain convergent solutions of q in 0.24 – 1.0, but the weighted sum of the squared residuals (hereafter \sum) in range 0.24 – 0.42 is larger than 10^{-3} , so only \sum in 0.42

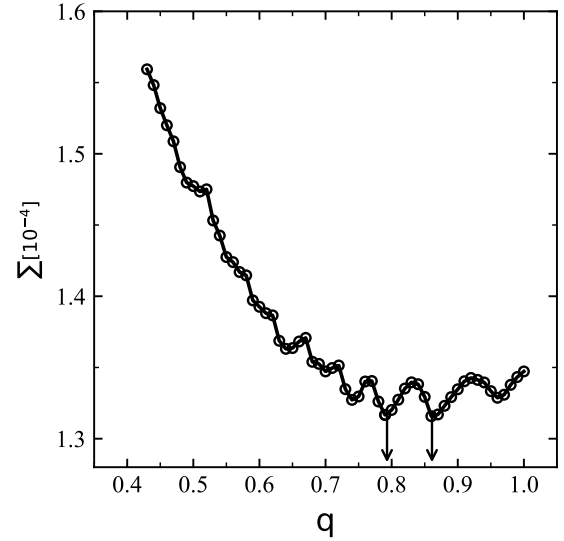


Fig. 4 Behavior of \sum (the weighted sum of the residuals squared) of KIC 5197256 as a function of mass ratio q , showing minimum values at $q \sim 0.861$ and $q \sim 0.793$. The *open circles* represent the q-search results for the detached configurations.

– 1.0 is presented. \sum versus q indicated that $q = 0.861$ is the minimum value. The q-search process is applied to different modes of W-D code, and only the detached mode 2 in which neither the primary nor secondary component is full of inner Roche lobe shows acceptable photometric solutions. This value is set as an initial guess and could be adjusted during the fitting procedure. In the second and third columns of Table 2, a possible photometric solution based on the light curve with pulsation is presented. The corresponding comparison of observed and theoretical light curves (from photometric solution) is shown in the top panel of Figure 2. By averaging the light curve in the whole phase according to the interval of bin = 0.001, we smooth it out to remove pulsation and leave the light variations owing to binary occultation. The light-curve fitting solution is listed in the fourth and fifth columns of Table 2 while the comparing plot is illustrated in the bottom panel of Figure 2. The differences in luminosity at the maxima times may be caused by the emergence of star spots, and we adopt the one spot or two spots mode in the W-D code during the light curve fitting. The latter one results in an inconspicuous improved fitting effect than the former, i.e., the \sum value of the latter is smaller, but the model convergence becomes difficult. So we only maintain the solutions with one spot as listed in Table 2.

By comparing the solutions of light curves with and without pulsation, it is obvious that they correspond with each other. The value of q is ~ 0.86 suggests that the mass of the primary is almost the same as that of the secondary. According to the spectral type A7V

Table 2 Photometric Solutions of KIC 5197256 with $q \sim 0.861$

Parameters	Best-fit Value(Pulsation)		Best-fit Value(No pulsation)	
	Primary	Secondary	Primary	Secondary
$g1 = g2$ (deg)		1.00		1.00
$A1 = A2$ (deg)		1.00		1.00
X_{bolo}	0.648	0.661	0.648	0.661
Y_{bolo}	0.239	0.252	0.239	0.252
x	0.639	0.647	0.639	0.647
y	0.290	0.286	0.290	0.286
i (deg)		20.49(6)		20.50(7)
$q=M_2/M_1$		0.861(1)		0.860(2)
T (K)	7830(fixed)	6920(18)	7830(fixed)	6919(21)
Ω	4.22(5)	4.21	4.22(3)	4.21
$L_1/(L_1 + L_2)$		0.720(4)		0.721(5)
r (pole)	0.2943(3)	0.2701(3)	0.2942(3)	0.2701(6)
r (side)	0.3016(5)	0.2761(4)	0.3016(6)	0.2760(5)
r (back)	0.3116(6)	0.2857(6)	0.3115(5)	0.2856(7)
Latitude _{spot} (deg)		87.89(0.51)		87.92(0.64)
Longitude _{spot} (deg)		41.60(1.93)		42.13(2.26)
Radius _{spot} (deg)		10.53(0.50)		10.71(0.49)
T_{spot}/T_2		0.957(1)		0.955(3)

Table 3 Photometric Solutions of KIC 5197256 with $q \sim 0.793$

Parameters	Best-fit Value(Pulsation)		Best-fit Value(No pulsation)	
	Primary	Secondary	Primary	Secondary
$g1 = g2$ (deg)		1.00		1.00
$A1 = A2$ (deg)		1.00		1.00
X_{bolo}	0.648	0.661	0.648	0.661
Y_{bolo}	0.239	0.252	0.239	0.252
x	0.639	0.647	0.639	0.647
y	0.290	0.286	0.290	0.286
i (deg)		23.23(5)		23.26(7)
$q=M_2/M_1$		0.793(2)		0.794(1)
T (K)	7830(fixed)	6944(22)	7830(fixed)	6943(31)
Ω	4.31(5)	4.22	4.31(4)	4.22
$L_1/(L_1 + L_2)$		0.724(6)		0.725(5)
r (pole)	0.2814(8)	0.2514(9)	0.2814(3)	0.2514(4)
r (side)	0.2873(6)	0.2561(8)	0.2872(3)	0.2561(2)
r (back)	0.2947(7)	0.2637(6)	0.2947(4)	0.2637(3)
Latitude _{spot} (deg)		88.32(0.57)		88.66(0.63)
Longitude _{spot} (deg)		40.79(1.53)		41.20(1.76)
Radius _{spot} (deg)		10.59(0.17)		10.51(0.14)
T_{spot}/T_2		0.957(2)		0.958(3)

providing by LAMOST, the mass of its companion main-sequence star is $\sim 1.84 M_{\odot}$. Then, we derive the mass of the secondary star is estimated to be $\sim 1.58 M_{\odot}$ with a corresponding temperature of ~ 7150 K (spectral type F1V), which is higher than the convergence value ~ 6920 K of light-curve fitting. The q -search results are all convergent solutions, so we adopt another minimum point with the second smallest \sum value, i.e., $q = 0.79$. The mass ratio of $q = 0.79$ is used as the initial guess during the light curve fitting and the results are in Table 2 and Figure 2, which are the same format of Table 3 and Figure 3. One can see that the q value converges to ~ 0.794 . The mass of the secondary star can be obtained as $\sim 1.55 M_{\odot}$ with the corresponding temperature ~ 6900 K (\sim F3V), which is close to the fitting values ~ 6940 K

listed in Table 3. Simultaneously, this is also consistent with the detached model because the material of two stars has not yet communicated with each other, the temperature characteristics of the main sequence stars.

For the temperatures provided by LAMOST DR7, they are driven by fitting sing-star models. In 2017, El-Badry et al. (2018) concluded that for the binary star with $3100 \text{ K} < T_{\text{eff}} < 7000 \text{ K}$ and $0.5 < q < 0.8$, the median error of spectral temperature of LAMOST-like spectra is less than that of APOGEE-like spectra which is 330 K. Although the spectral temperature of the primary star of KIC 5197256 is 7830 K, which is not within this study, it is reasonable for us to apply 330 K as temperature error to KIC 5197256 in the absence of other recent error estimates. We also further amplify the temperature

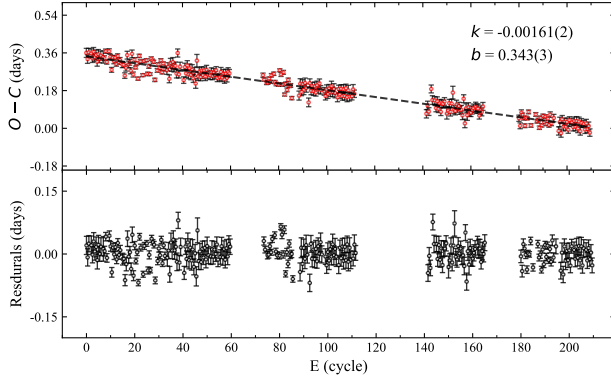


Fig. 5 The $O - C$ diagram for KIC 5197256. Observed data are plotted in *red circles*, while the *black dashed line* represents the linear fit to the data (*top panel*). The bottom panel shows the residuals between the observed data and the fitting data.

error of secondary and employ ± 330 K. Therefore, the temperature of two components is $7830 \text{ K} \pm 330 \text{ K}$ and $6940 \text{ K} \pm 330 \text{ K}$. Combining the Kepler Eclipsing Binary Catalogue (KEBC; Prša et al. 2011; Slawson et al. 2011; Matijevič et al. 2012) with the information collected from the Howell-Everett Survey (HES), Kepler INT Survey (KIS; Greiss et al. 2012) and 2MASS (Skrutskie et al. 2006), Armstrong et al. (2014) developed spectral energy distribution fits which can be used to determine stellar temperatures of components of eclipsing binary stars. Our results of the temperature difference between two components $\Delta T \approx 900 \text{ K}$ is almost consistent with the temperature difference derived by them, i.e., $\sim 1000 \text{ K}$ (final primary star T_1 as $8200 \text{ K} \pm 366 \text{ K}$ and final secondary star T_2 as $7142 \text{ K} \pm 599 \text{ K}$). For the inclination i of KIC 5197256 in Table 3, its value is $\sim 23^\circ$, which is a very low angle relative to other close binaries. However, one should note that the magnitude difference at the time of the eclipsing of this source is very small, i.e., $\sim 10 \text{ mmag}$, so the angle value is reasonable.

3.2 The $O - C$ Analysis

We construct a classical $O - C$ diagram to exam the prospective long-term period variation of KIC 5197256. O is the observed minimum light time, and C is the theoretical value in the ephemeris equation (Sterken 2005). For the calculations of O , an initial visual inspection of the light curve is conducted to determine the minimum time, then made a parabolic fitting of the light curve to obtain the original minimum. A total of 265 minimum times are used in the analysis of $O - C$. Then $O - C$ values are calculated by Equation (1). T_0 is the initial epoch, P is the period, and

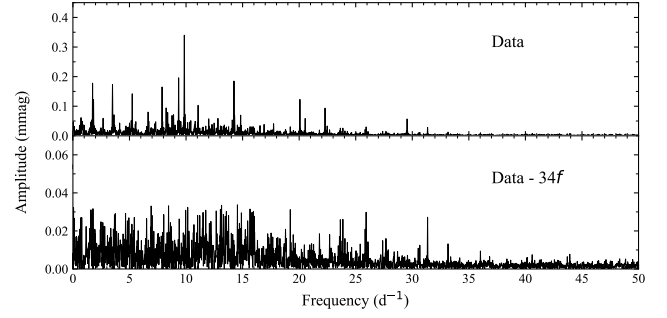


Fig. 6 Amplitude spectra before (top panel) and after pre-whitening all 34 frequencies (bottom panel) from the PERIOD04 program for all light residuals.

E is the cycle number.

$$\begin{aligned} T_{\min} &= T_0 + P \times E \\ &= 2454954.3625(4) + 6.9650(1) \times E, \end{aligned} \quad (1)$$

the $O - C$ values are then obtained from this ephemeris equation. All the values of $O - C$ and the corresponding number of cycles are listed in Table 6.

As seen in the top panel of Figure 5, the $O - C$ diagram is a straight line with a negative slope which means that its period is almost constant over a period of at least 2 yr. The corresponding residual $O - C$ is shown in the bottom panel of Figure 5, suggesting no clear period change to be observed. There is no change in the period, indicating that the amount of mass transferred between the two stars is relatively small and the current state of two stars is relatively stable (Panchal & Joshi 2021). Alternatively, it is possible that the observations of this star are not long enough for the period variation to be reflected. Equation (2) is the update epoch formula.

$$\begin{aligned} T_{\min} &= T_0 + P \times E \\ &= 2454954.337(2) + 6.96341(2) \times E. \end{aligned} \quad (2)$$

4 FREQUENCY ANALYSIS

We performed a Fourier analysis of the corrected data using PERIOD04 (Lenz & Breger 2005) to study the pulsation behavior of the residuals after removing the binary effects. The frequency range we choose is $0 < \nu < 50 \text{ d}^{-1}$, which is somewhat wider than the typical pulsation frequency of δ Sct stars, for more significant frequency detection in the SC data. The two frequencies are considered to be resolved if the difference between frequencies is larger than the resolution frequency $f_{\text{res}} = 1 / T$, which is 0.034 d^{-1} for the SC light curve of KIC 5197256. To extract the significant frequencies, the highest peak in the frequency spectrum is assumed to be the significant frequency in the process of extracting, and

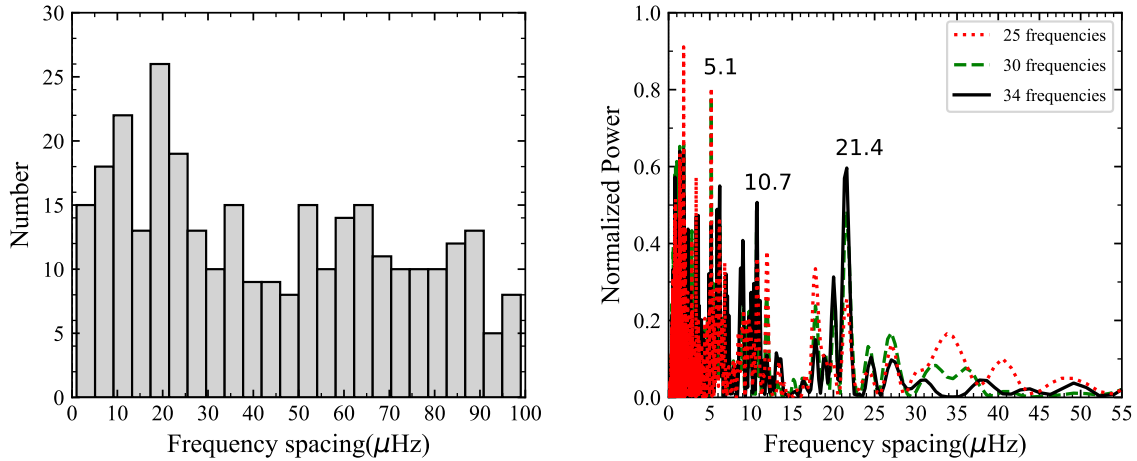


Fig. 7 The distribution of the frequency differences between each two pulsation frequencies is shown in the left panel. The Fourier transform of 34 pulsation frequencies (*solid line*), 30 pulsation frequencies (*dashed line*) and 25 pulsation frequencies (*dotted line*) are shown in the right panel. The regular frequency spacing detailed analyses are described in Sect. 4.1.

then a multi-frequency least-squares fit is performed using the formula:

$$m = m_0 + \sum_{i=1}^N A_i \sin(2\pi(f_i t + \phi_i)). \quad (3)$$

The light curve is examined for all significant frequencies and the solutions for all significant frequencies are derived, where m_0 denotes the zero point, A_i is the amplitude, f_i is the frequency, and ϕ_i is the corresponding phase. All frequencies of combination frequencies are fixed to exact values that are supposed to be and only leave the independent frequencies, all amplitudes, and all phases as free parameters to be improved. The constructed light curve was subtracted from the data using the above solutions, and the residual was obtained to search for a significant signal in the next step. Then the steps were repeated until there were no significant peaks in the residuals. The criterion ($S/N > 3.5$) proposed by Breger et al. (2011) was used to determine the significant peaks. The uncertainties of frequencies are calculated following Kallinger et al. (2008).

There are 34 significant frequencies extracted and listed in Table 4. The amplitude spectra of all 34 frequencies and after pre-whitening are shown in the top and bottom panels of Figure 6. Some additional peaks still exist in the bottom panel of Figure 6, but their S/N ratios are smaller than the empirical threshold of 3.5. As shown in Figure 6, most of the detected frequencies lie in a region between 5 and 30 d^{-1} . With the dominant peak at $f_1 = 9.84 \text{ d}^{-1}$ and several independent frequencies, the linear combination frequencies can be expressed very simply through the equation $f = m f_1 \pm n f_2$, where m and n are small integers. These frequencies are all listed in Table 4 with different notes. Five frequencies have

been detected in the range of 1 – 5 d^{-1} (f_4, f_5, f_{10}, f_{17} and f_{22}). The frequency f_4 was considered as a multiple of the orbital frequency, while f_{22} was considered as a combination frequency of f_1 and f_2 . Obviously f_5 and f_{17} are the harmonics of f_4 and f_{10} respectively. The remained frequency f_{10} cannot be combinations of any other frequencies.

Identifying the value of the pulsation mode l is quite difficult when analyzing pulsating variable stars. Usually, pulsation modes can be identified by comparing the phase lag between the light curves of different wavelengths (Breger et al. 1999; Páparó et al. 2018). Another method is to analyze the spectroscopic equivalent width and intensity because different mode values will cause different variations (Bedding et al. 1996; Balona 2000). Although KIC 5197256 does not have any multi-color photometry and high-resolution spectroscopic observations, some useful information could be obtained from the frequencies spectrum analysis. Large frequency separations have been founded by Bedding et al. (2020), suggesting a correlation between the large separation and the rotation of the star with regular spacing.

4.1 Regular Frequency Spacing

To find the regular spacing of δ Sct stars, there are several mature methods such as the histogram graph (Breger et al. 1999), and the Fourier transform method (García Hernández et al. 2009, 2013, 2015). We first use the histogram graph method to search for the regular spacing. Calculate the frequency difference between every two of the 34 extracted frequencies. The distribution of the frequency differences is presented in Figure 7. The bin size of the histogram graph is 4 μHz (1 d^{-1}

Table 4 Extracted Frequencies in SC Data of KIC 5197256

ID	Frequency (d^{-1})	Amplitude (mmag)	Phase (rad)	S/N	Note
f_1	9.8465 ± 0.0001	0.335 ± 0.002	0.8211 ± 0.0013	16.22	...
f_2	9.3433 ± 0.0002	0.191 ± 0.002	0.2229 ± 0.0023	11.06	...
f_3	14.2372 ± 0.0002	0.183 ± 0.002	0.9298 ± 0.0024	9.66	...
f_4	1.7379 ± 0.0002	0.166 ± 0.002	0.2620 ± 0.0026	10.82	$12f_{orb}$
f_5	3.4983 ± 0.0002	0.174 ± 0.002	0.8440 ± 0.0025	11.37	$24f_{orb}$
f_6	7.8803 ± 0.0002	0.166 ± 0.002	0.4818 ± 0.0026	8.94	...
f_7	5.2432 ± 0.0002	0.144 ± 0.002	0.1470 ± 0.0030	10.95	$36f_{orb}$
f_8	20.0649 ± 0.0002	0.124 ± 0.002	0.6717 ± 0.0035	16.74	...
f_9	11.0640 ± 0.0003	0.109 ± 0.002	0.0315 ± 0.0040	6.30	...
f_{10}	1.8192 ± 0.0003	0.103 ± 0.002	0.0896 ± 0.0042	7.75	f_{rot}
f_{11}	22.2854 ± 0.0004	0.095 ± 0.002	0.1364 ± 0.0046	16.72	...
f_{12}	8.2400 ± 0.0004	0.092 ± 0.002	0.4360 ± 0.0047	5.44	...
f_{13}	6.6456 ± 0.0004	0.084 ± 0.002	0.0391 ± 0.0052	7.14	...
f_{14}	8.3766 ± 0.0004	0.078 ± 0.002	0.0452 ± 0.0056	5.51	...
f_{15}	8.7606 ± 0.0005	0.072 ± 0.002	0.3199 ± 0.0061	5.26	...
f_{16}	14.8269 ± 0.0005	0.071 ± 0.002	0.9685 ± 0.0061	5.68	...
f_{17}	3.6349 ± 0.0005	0.072 ± 0.002	0.8791 ± 0.0060	4.71	$2f_{rot}$
f_{18}	8.8954 ± 0.0005	0.070 ± 0.002	0.4821 ± 0.0063	5.77	...
f_{19}	20.5301 ± 0.0005	0.062 ± 0.002	0.3656 ± 0.0070	12.03	...
f_{20}	0.7193 ± 0.0005	0.062 ± 0.002	0.8585 ± 0.0070	4.14	$2f_1-2f_2-2f_{orb}$
f_{21}	12.8175 ± 0.0006	0.060 ± 0.002	0.5549 ± 0.0072	3.81	...
f_{22}	2.6665 ± 0.0006	0.058 ± 0.002	0.6638 ± 0.0076	4.82	$f_1-f_2+15f_{orb}$
f_{23}	25.9186 ± 0.0007	0.0568 ± 0.002	0.8448 ± 0.0085	5.06	...
f_{24}	29.5397 ± 0.0006	0.0567 ± 0.002	0.4659 ± 0.0077	17.81	$3f_1$
f_{25}	12.0047 ± 0.0006	0.0541 ± 0.002	0.3442 ± 0.0081	3.96	...
f_{26}	10.8063 ± 0.0007	0.0507 ± 0.002	0.8712 ± 0.0086	3.54	...
f_{27}	5.5544 ± 0.0007	0.0485 ± 0.002	0.6435 ± 0.0090	4.04	...
f_{28}	9.5370 ± 0.0007	0.0465 ± 0.002	0.7508 ± 0.0094	4.03	f_1-2f_{orb}
f_{29}	10.3757 ± 0.0007	0.0459 ± 0.002	0.6751 ± 0.0095	3.66	$2f_1-f_2$
f_{30}	7.3166 ± 0.0007	0.0455 ± 0.002	0.7940 ± 0.0096	3.65	...
f_{31}	7.2526 ± 0.0008	0.0437 ± 0.002	0.7053 ± 0.0101	4.11	...
f_{32}	31.3505 ± 0.0012	0.0271 ± 0.002	0.8832 ± 0.0161	9.99	...
f_{33}	27.6709 ± 0.0021	0.0159 ± 0.002	0.0333 ± 0.0273	4.77	...
f_{34}	33.1556 ± 0.0025	0.0133 ± 0.002	0.3584 ± 0.0327	5.79	...

= 11.57 μHz). Two significant peaks are found near 11 μHz and 20 μHz . The first peak is at 11 μHz may be caused by the close frequencies and the potential rotational splitting frequency. The second significant peak is near 20 μHz and may be explained by large separations at frequencies of different radial orders of the same degree l , or by rotationally induced frequency splitting. The Fourier transform is another well-studied method for exploring regular frequency spacings. We follow the descriptions of García Hernández et al. (2009) to obtain the frequency spacing for KIC 5197256. Dirac's Delta Function with equal amplitudes is considered as a series of extracted frequencies. The Fourier transform of these frequencies is then calculated. We give the Fourier transforms of the highest 25 and 30 and 34 frequencies as a comparison, as shown in Figure 8. A periodic pattern is identified at all 34 frequencies. Significant peaks appear around 5.1, 10.7, and 21.4 μHz . Compared with the results of the histogram graph method, it indicates that there may be regular frequency spacing around 21 μHz .

4.2 The Mean Stellar Density

The average stellar density is theoretically predicted to be proportional to the large separation of δ Sct stars (Suárez

et al. 2014). A similar conclusion is revealed by examining some eclipse binary systems with δ Sct components (García Hernández et al. 2015), and the large separation-mean density ($\Delta\nu - \rho$) relation is also appropriate for eclipsing binaries (Streamer et al. 2018). The relationship was refined by implementing a Hierarchical Bayesian linear regression method (García Hernández et al. 2017). Updated large separation-mean and density ($\Delta\nu - \rho$) relation is :

$$\bar{\rho}/\bar{\rho}_{\odot} = 1.50_{-0.10}^{+0.09} (\Delta\nu/\Delta\nu_{\odot})^{2.04_{-0.04}^{+0.04}}, \quad (4)$$

where $\Delta\nu_{\odot} = 134.8 \mu\text{Hz}$ (Kjeldsen et al. 2008), so the average density is $0.05 \text{ g}\cdot\text{cm}^{-3}$ for δ Sct companion of KIC 5197256 using this formula and a large separation value of 21 μHz . As shown in Figure 9, the $\log(\rho/\rho_{\odot})$ is plotted as a function of the $\log(\Delta\nu/\Delta\nu_{\odot})$, and KIC 5197256 is overplotted with a blue star. The other data (black circle) are taken from García Hernández et al. (2017) and García Hernández et al. (2015) while the red line represents the linear fitting using a Bayesian method. The slope and the offset are estimated as $k = 0.14 \pm 0.01$ and $b = 1.97 \pm 0.02$, which are consistent with those given by García Hernández et al. (2017) within the quoted errors.

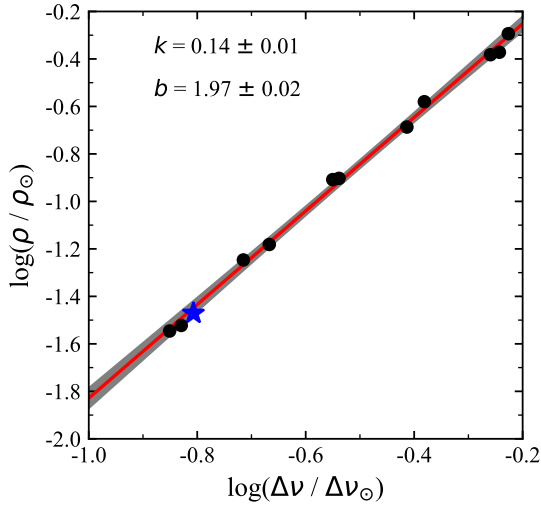


Fig. 8 $\Delta\nu - \bar{\rho}$ relation calculated using Bayesian method. The *blue star* indicates KIC 5197256 and the other data (*black circle*) are from García Hernández et al. (2017) and García Hernández et al. (2015). The slope and the offset are estimated as $k = 0.14 \pm 0.01$ and $b = 1.97 \pm 0.02$.

5 DISCUSSION

5.1 Eclipsing or Ellipsoidal Variable

The ellipsoidal variable stars are binaries that do not eclipse and are incredibly close binaries (Morris 1985; Beech 1985). For ellipsoidal variable stars, the inclination (i) of the binary is so small that the system does not show any eclipses. The variation is mainly due to the components with non-spherical shapes. KIC 5197256 has the same characteristic, which is consistent with ellipsoidal variable stars. Fourier analysis is utilized to determine whether KIC 5197256 is an elliptical variable star. According to Morris (1985); Beech (1985) and Morris & Naftilan (1993), whereas Fourier analysis can model the light curve of ellipsoidal variable stars if the main variation is indeed due to ellipsoidal effect i.e., ellipsoidal variable star light curves can be modeled by the Fourier analysis given by Equation (5), and the $\cos(2\theta)$ term should be dominated among all other terms in the results of the Fourier analysis, which is of modern methods utilized in previous studies, like Faigler & Mazeh (2011) and Faigler et al. (2012).

$$L(\theta) = A_0 + \sum_{i=1}^N A_i \cos(i\theta) + \sum_{i=1}^N B_i \sin(i\theta), \quad (5)$$

suppose the $\cos(2\theta)$ term is the dominant component over all other terms in Fourier analysis results. In that case, the primary effect of light variation is the ellipsoidal effect (Dal & Sipahi 2013). Thus we can take the Fourier analysis

Table 5 The Additional $\ell = 2$ Quintuplet: Observed Separation

Frequency (d^{-1})	Separation from central frequency (d^{-1})
Quintuplet	
25.919 ± 0.001	-3.620 ± 0.001
27.671 ± 0.002	-1.868 ± 0.001
29.539 ± 0.001	0 ± 0.001
31.351 ± 0.001	1.812 ± 0.001
33.155 ± 0.003	3.616 ± 0.002

equation as follows:

$$L(\theta) = A_0 + A_1 \cos(\theta) + B_1 \sin(\theta) + A_2 \cos(2\theta) + B_2 \sin(2\theta), \quad (6)$$

The coefficients derived from the Fourier model are as follows: $A_0 = 0.000527(5)$; $A_1 = -0.004227(7)$; $B_1 = -0.148(4)$; $A_2 = 0.00509(7)$; $B_2 = 0.073(2)$. The \cos component coefficient A_2 is significantly smaller than that of the \sin component, suggesting that KIC 5197256 could not be an ellipsoidal variable.

5.2 The Quintuplet

The pulsation amplitudes of δ Sct stars increase as the rotation decreases (e.g., see fig. 5 of Breger & Montgomery (2000)). Radial pulsators with slow rotation generally generate high amplitude frequencies. KIC 5197256 is a star with low-amplitude non-radial modes. Suggesting that KIC 5197256 might have a relatively large rotational velocity, and a dominant frequency with low amplitude (i.e., ~ 0.3345). During the Kepler mission, several δ Sct stars were found to show equidistant multiplets in their frequency spectra, which are caused by amplitude modulation of the stellar rotation (Breger et al. 2011), and low amplitude modulation frequencies with splitting frequency values of 0.16 d^{-1} are detected around the dominant pulsation frequency of KIC 9700322, which was identified by high dispersion spectroscopic observations as the stellar rotation frequency (Breger et al. 2011). A pair of equidistant side peaks around the main frequency also has been found in the frequency spectrum of a HADS star KIC 5950759 (Yang et al. 2018), and the authors suggest that the frequency split is caused by stellar rotation. They also detected two frequencies considered as the amplitude modulation with two dominant frequencies (Yang & Esamdin 2019). The periodic variation of the amplitudes of the two dominant pulsation modes suggests that the modulation of KIC 10284901 may be related to the Blazhko effect. These are examples of amplitude modulation on the dominant frequency by a frequency in the low-frequency region. In the frequency region of 25 to 34 d^{-1} , we detect a multiplet in the frequency spectrum on either side of $3f_1$ (29.539 d^{-1}), which is listed in Table 5, and this multiplet has a mean separation $\Delta f_{\text{mean}} = 1.81 \text{ d}^{-1}$, which is different from the case of

Table 6 265 Times of Minimum Light and $O - C$ Values of KIC 5197256

BJD (2400000+)	E	$O - C$ (d)	Error (d)	BJD (2400000+)	E	$O - C$ (d)	Error (d)
54954.36247	0	0.363	0.011	55584.51934	90.5	0.187	0.014
54957.81568	0.5	0.333	0.016	55588.03381	91	0.219	0.019
54961.32998	1	0.365	0.010	55591.49243	91.5	0.195	0.014
54968.28964	2	0.36	0.011	55598.38873	92.5	0.126	0.017
54971.7489	2.5	0.336	0.015	55601.96355	93	0.219	0.012
54975.26213	3	0.367	0.011	55605.40969	93.5	0.182	0.019
54978.72005	3.5	0.343	0.016	55608.91347	94	0.203	0.012
54982.21244	4	0.353	0.012	55612.37256	94.5	0.18	0.015
54985.66288	4.5	0.32	0.017	55615.87811	95	0.203	0.019
54989.18083	5	0.356	0.011	55619.33049	95.5	0.173	0.010
54992.64092	5.5	0.334	0.015	55622.84819	96	0.208	0.015
54996.13979	6	0.35	0.012	55626.31197	96.5	0.189	0.009
55003.09802	7	0.343	0.022	55629.82102	97	0.216	0.016
55006.57435	7.5	0.337	0.012	55633.2738	97.5	0.186	0.010
55010.09065	8	0.371	0.008	55643.71375	99	0.179	0.013
55013.52165	8.5	0.319	0.013	55647.17476	99.5	0.157	0.010
55020.53792	9.5	0.371	0.023	55650.68781	100	0.188	0.016
55023.99432	10	0.344	0.013	55654.14914	100.5	0.167	0.012
55027.41407	10.5	0.282	0.008	55657.6582	101	0.193	0.017
55030.95476	11	0.34	0.013	55661.12231	101.5	0.175	0.010
55034.42031	11.5	0.323	0.007	55664.63311	102	0.203	0.015
55037.91935	12	0.339	0.012	55668.08893	102.5	0.176	0.011
55041.37187	12.5	0.309	0.007	55671.58569	103	0.191	0.017
55044.89269	13	0.348	0.011	55675.04886	103.5	0.171	0.010
55048.3459	13.5	0.318	0.007	55681.9922	104.5	0.15	0.017
55051.83884	14	0.329	0.012	55685.5152	105	0.19	0.012
55058.78099	15	0.306	0.007	55688.97188	105.5	0.164	0.018
55062.26348	15.5	0.306	0.012	55692.48124	106	0.191	0.013
55065.69417	16	0.254	0.008	55695.92905	106.5	0.157	0.018
55072.75659	17	0.352	0.010	55699.4441	107	0.189	0.015
55076.1953	17.5	0.308	0.010	55702.89395	107.5	0.156	0.009
55079.68755	18	0.318	0.013	55706.41367	108	0.194	0.015
55083.12951	18.5	0.277	0.008	55709.85393	108.5	0.151	0.009
55086.6927	19	0.358	0.011	55713.36876	109	0.184	0.014
55090.07673	19.5	0.259	0.008	55716.82186	109.5	0.154	0.011
55093.63015	20	0.33	0.016	55723.78826	110.5	0.156	0.037
55097.07525	20.5	0.293	0.018	55727.3031	111	0.188	0.028
55100.57759	21	0.313	0.016	55730.76504	111.5	0.168	0.043
55103.9871	21.5	0.24	0.011	55939.6194	141.5	0.072	0.029
55107.57812	22	0.348	0.011	55943.14215	142	0.112	0.040
55111.03402	22.5	0.322	0.008	55946.59496	142.5	0.082	0.034
55117.93382	23.5	0.256	0.013	55953.66803	143.5	0.19	0.027
55121.4832	24	0.323	0.008	55957.09734	144	0.137	0.033
55128.45256	25	0.328	0.012	55964.06063	145	0.136	0.038
55131.86968	25.5	0.262	0.011	55967.50661	145.5	0.099	0.024
55135.38862	26	0.299	0.009	55971.02163	146	0.132	0.015
55138.83385	26.5	0.261	0.010	55974.46815	146.5	0.096	0.022
55142.39034	27	0.335	0.008	55977.97686	147	0.122	0.011
55145.86395	27.5	0.327	0.014	55981.41877	147.5	0.081	0.021
55149.33974	28	0.32	0.010	55984.93992	148	0.12	0.009
55152.73618	28.5	0.234	0.011	55988.42164	148.5	0.119	0.015
55159.746	29.5	0.279	0.008	55991.91595	149	0.131	0.010
55163.25746	30	0.308	0.009	55998.82288	150	0.073	0.015
55166.72306	30.5	0.291	0.007	56002.32034	150.5	0.088	0.009
55170.24144	31	0.327	0.012	56005.83766	151	0.123	0.014
55173.66736	31.5	0.27	0.014	56009.27872	151.5	0.081	0.010
55177.19189	32	0.312	0.008	56012.80072	152	0.121	0.021
55180.64833	32.5	0.286	0.013	56016.33541	152.5	0.173	0.010
55187.60719	33.5	0.28	0.008	56019.7373	153	0.092	0.014
55191.10635	34	0.296	0.013	56023.21283	153.5	0.085	0.013
55194.53126	34.5	0.239	0.008	56026.72645	154	0.116	0.009
55198.08879	35	0.314	0.015	56030.19059	154.5	0.098	0.018
55201.55138	35.5	0.294	0.015	56033.684	155	0.109	0.011
55205.05888	36	0.319	0.010	56037.14708	155.5	0.09	0.018
55208.51522	36.5	0.293	0.016	56040.63117	156	0.091	0.011
55212.00546	37	0.301	0.012	56044.08737	156.5	0.065	0.014

Table 6 Continued.

BJD (2400000+)	E	$O - C$ (d)	Error (d)	BJD (2400000+)	E	$O - C$ (d)	Error (d)
55215.45123	37.5	0.264	0.016	56047.64885	157	0.144	0.010
55219.03192	38	0.362	0.011	56051.01352	157.5	0.026	0.014
55222.41285	38.5	0.26	0.017	56054.56777	158	0.098	0.008
55225.93188	39	0.297	0.011	56058.01752	158.5	0.065	0.015
55236.31511	40.5	0.233	0.017	56061.5388	159	0.104	0.010
55239.85964	41	0.295	0.009	56065.00084	159.5	0.083	0.016
55243.3118	41.5	0.264	0.016	56068.47696	160	0.077	0.010
55246.83287	42	0.303	0.011	56071.9725	160.5	0.09	0.016
55250.27268	42.5	0.26	0.013	56075.46352	161	0.098	0.011
55253.78373	43	0.289	0.010	56082.43468	162	0.105	0.020
55257.23482	43.5	0.257	0.015	56085.90892	162.5	0.096	0.010
55260.74276	44	0.283	0.012	56089.39143	163	0.096	0.017
55264.18313	44.5	0.241	0.019	56092.84095	163.5	0.063	0.009
55267.69722	45	0.272	0.010	56096.34863	164	0.089	0.014
55271.12394	45.5	0.216	0.018	56099.82349	164.5	0.081	0.009
55274.71545	46	0.325	0.012	56103.33203	165	0.107	0.012
55278.12373	46.5	0.251	0.015	56207.75059	180	0.051	0.018
55281.62816	47	0.273	0.010	56211.19707	180.5	0.014	0.011
55285.08491	47.5	0.247	0.019	56214.74298	181	0.078	0.013
55288.59834	48	0.278	0.016	56218.21449	181.5	0.067	0.021
55292.05917	48.5	0.257	0.015	56221.6813	182	0.051	0.030
55295.5639	49	0.279	0.009	56225.12743	182.5	0.015	0.018
55299.01783	49.5	0.25	0.014	56228.64801	183	0.053	0.022
55302.5314	50	0.281	0.009	56232.12734	183.5	0.05	0.037
55305.99147	50.5	0.259	0.013	56235.64095	184	0.081	0.021
55312.95227	51.5	0.255	0.009	56242.54127	185	0.016	0.024
55316.45058	52	0.271	0.015	56256.52373	187	0.069	0.016
55319.91493	52.5	0.252	0.010	56259.97336	187.5	0.036	0.026
55323.41352	53	0.269	0.016	56263.46207	188	0.042	0.015
55326.88477	53.5	0.257	0.015	56266.90789	188.5	0.005	0.014
55330.38909	54	0.279	0.010	56270.43774	189	0.053	0.010
55333.83459	54.5	0.242	0.013	56273.88419	189.5	0.017	0.016
55340.80428	55.5	0.247	0.009	56277.4119	190	0.062	0.009
55344.3116	56	0.272	0.014	56280.86527	190.5	0.033	0.023
55347.76701	56.5	0.245	0.009	56284.37369	191	0.059	0.009
55351.26802	57	0.263	0.013	56287.82072	191.5	0.023	0.014
55354.72448	57.5	0.237	0.013	56291.32914	192	0.049	0.009
55358.2337	58	0.264	0.010	56294.78039	192.5	0.018	0.013
55361.69561	58.5	0.243	0.015	56298.31317	193	0.068	0.009
55365.20687	59	0.272	0.010	56301.75384	193.5	0.026	0.014
55368.68243	59.5	0.265	0.015	56308.74398	194.5	0.051	0.008
55466.18382	73.5	0.256	0.010	56322.61259	196.5	-0.01	0.013
55469.64479	74	0.235	0.016	56326.1376	197	0.032	0.009
55476.5954	75	0.22	0.018	56329.5671	197.5	-0.021	0.012
55480.07814	75.5	0.221	0.026	56333.11585	198	0.046	0.009
55483.57976	76	0.24	0.031	56336.56314	198.5	0.011	0.015
55487.04707	76.5	0.225	0.015	56340.06828	199	0.033	0.010
55490.56061	77	0.256	0.020	56343.52804	199.5	0.01	0.013
55497.53302	78	0.263	0.024	56347.03318	200	0.033	0.013
55500.9757	78.5	0.223	0.016	56350.47825	200.5	-0.004	0.015
55504.44873	79	0.214	0.020	56354.00637	201	0.041	0.011
55511.41105	80	0.211	0.016	56360.96078	202	0.031	0.015
55514.96215	80.5	0.28	0.008	56364.42181	202.5	0.009	0.009
55518.42461	81	0.26	0.012	56367.93219	203	0.037	0.016
55521.85909	81.5	0.212	0.008	56371.38756	203.5	0.01	0.009
55525.39985	82	0.27	0.012	56374.89717	204	0.037	0.013
55528.77613	82.5	0.164	0.009	56378.34452	204.5	0.002	0.008
55532.30942	83	0.214	0.012	56381.85999	205	0.035	0.012
55535.76331	83.5	0.186	0.009	56385.29604	205.5	-0.012	0.008
55539.29362	84	0.234	0.013	56388.81864	206	0.029	0.016
55542.74752	84.5	0.205	0.008	56395.77839	207	0.023	0.009
55546.23221	85	0.207	0.011	56399.23461	207.5	-0.003	0.015
55549.65417	85.5	0.147	0.012	56402.74597	208	0.026	0.010
55570.56116	88.5	0.159	0.019	56406.20119	208.5	-0.001	0.016
55574.10061	89	0.216	0.011	56409.69852	209	0.013	0.010
55577.54385	89.5	0.176	0.014	56413.14973	209.5	-0.018	0.015
55581.06352	90	0.214	0.010				

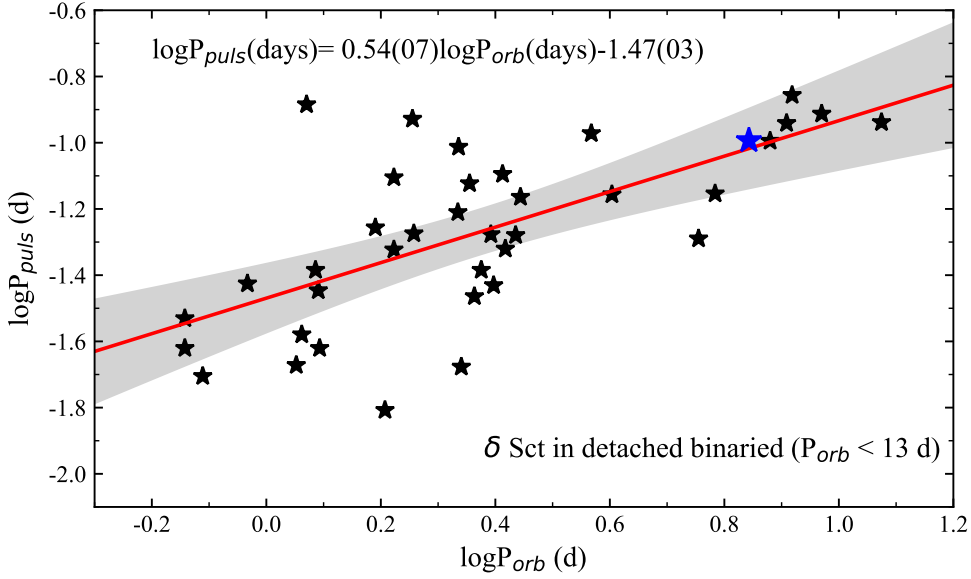


Fig. 9 Location of the oscillating (primary) component of KIC 5197256 (*blue star*) among other δ Scuti stars-members (*black stars*) of detached systems $P_{\text{orb}} < 13$ d within $P_{\text{orb}} - P_{\text{pul}}$ diagram, while the *solid line* denotes the empirical linear fitting through Monte Carlo simulation.

KIC 9700322, where the splitting occurs at the dominant frequency.

According to calibration of MK spectral types (Cox 2000), it is possible to obtain the rotation velocity $v \sin i \sim 150 \text{ km s}^{-1}$ corresponding to A7V star due to the previously obtained regular frequency spacing (i.e., $f_{10} = 1.8 \text{ d}^{-1}$). The frequency spacing $\Delta f_{\text{mean}} = 1.81$ in a regular pattern could not be modelled perfectly symmetrical in a second-order rotational effects (Saio 1981). Therefore the first-order approximation proposed by Saio et al. (2015) is adopted:

$$\langle P_{\text{rot}} \rangle = \frac{1}{\Delta f_{\text{rot}}} (1 - C_{n,\ell}), \quad (7)$$

where $C_{n,\ell}$ is the Ledoux constant (Ledoux 1951). The Ledoux constant $C_{n,\ell}$ is zero for p modes, and the rotation period is independent of the mode degree ℓ . Corresponds to a rotation period of 1.81 d^{-1} splitting equal to $P_{\text{rot}} = 0.552 \text{ d}$. Table 1 shows the R values derived from blended photometry. Both components, as we know, have similar atmospheric properties, so the value can be assumed to be a reasonable estimate for each system component. If consider the radius $R = 2.321 R_{\odot}$ as an estimation of the radius for one component, we could obtain equatorial velocities $v_{\text{eq}} \sim 209 \text{ km s}^{-1}$ for the star, based on 1.81 d^{-1} splitting. Considering a simple linear model of a classical δ Sct star with a mass and radius to be $M = 1.8 M_{\odot}$ and $R = 2 R_{\odot}$, a rotational splitting of $\sim 0.5 \text{ d}^{-1}$ could be produced with a slow rotator of $v \sin i \sim 50 \text{ km s}^{-1}$, while a rotational splitting of $\sim 1.0 \text{ d}^{-1}$ could be produced with a moderate rotator of $v \sin i \sim 100 \text{ km s}^{-1}$, and a rotational

splitting of $\sim 2.0 \text{ d}^{-1}$ could be produced with a fast rotator of $v \sin i \sim 200 \text{ km s}^{-1}$ (Bowman 2017).

So we consider that 1.81 d^{-1} might be caused by rotation similar to KIC 8975515 (Samadi-Ghadim et al. 2020). However, to obtain a more accurate value of $v \sin i$, a high-dispersion spectral analysis is required to derive it.

6 CONCLUSIONS

We have presented *Kepler* photometry of KIC 5197256, an eclipsing binary system KIC 5197256 with a δ Sct variable component. Through the $O - C$ analysis we obtained the period of KIC 5197256 is almost constant over about 2 yr. The large frequency separation is cross-identified with the histogram graph and the Fourier transform method. Based on the large separation and density relationship, the mean density of the δ Sct component is estimated to be 0.05 g cm^{-3} . Through Fourier analysis, a total of 34 significant frequencies are extracted.

Although there are no RVs for KIC 5197256, the absolute parameters of components also could be estimated under reasonable assumptions by software ABSPAREEB (Liakos 2015). The luminosities, gravity acceleration, and bolometric magnitudes of the primary star in KIC 5197256 are estimated as $75.519 \pm 13.3 L_{\odot}$, $3.352 \pm 0.045 \text{ cgs}$ and $0.055 \pm 1.019 \text{ mag}$ while those of the secondary star are estimated as $25.915 \pm 5.164 L_{\odot}$, $3.537 \pm 0.07 \text{ cgs}$ and $1.216 \pm 1.147 \text{ mag}$. Then, we examined the evolutionary state of KIC 5197256 in mass-luminosity, and Hertzsprung-Russell (HR) diagrams (Ibanoğlu et al.

2006; Lee & Park 2018). In these diagrams, the pulsating primary star is a slight deviation from the blue line of the δ Sct instability strip on the main-sequence band, while the low-mass companion resides within the δ Sct instability strip. Both companions are located in the pulsation instability strip, mainly because they have a relatively similar temperature. With the transfer of mass between the two components of KIC 5197256, the mass ratio will decrease, while $J_{\text{spin}}/J_{\text{orb}}$ increases. The binary could merge into a single rapidly rotating star, while the system reaches a state of $J_{\text{orb}} = 3J_{\text{spin}}$, because tidal instability will occur (Arbutina 2007). Figure 9 present the location of oscillating (primary) component of KIC 5197256 (blue star) among other δ Sct stars from Liakos (2020) (black stars) of detached systems $P_{\text{orb}} < 13$ d, while the solid line denotes the empirical linear fitting through Monte Carlo simulation suggesting that KIC 5197256 is a normal detached binary with a δ Sct component.

Acknowledgements This research is supported by the National Natural Science Foundation of China (Grant No. U2031209). We would like to thank the *Kepler* science team for providing such excellent data.

References

- Armstrong, D. J., Gómez Maqueo Chew, Y., Faedi, F., et al. 2014, *MNRAS*, 437, 3473
- Arbutina, B. 2007, *MNRAS*, 377, 1635
- Bowman, D. M. 2017, *Amplitude Modulation of Pulsation Modes in Delta Scuti Stars*, (Springer International Publishing), doi:10.1007/978-3-319-66649-5
- Balona, L. A. 2000, *MNRAS*, 319, 606
- Balona, L. A. 2014, *MNRAS*, 437, 1476
- Balona, L. A., & Dziembowski, W. A. 2011, *MNRAS*, 417, 591
- Bedding, T. R., Kjeldsen, H., Reetz, J., & Barbuy, B. 1996, *MNRAS*, 280, 1155
- Bedding, T. R., Murphy, S. J., Hey, D. R., et al. 2020, *Nature*, 581, 147
- Beech, M. 1985, *Ap&SS*, 117, 69
- Borucki, W. J., et al. 2010, *Science*, 327, 977
- Bowman, D. M., et al. 2016, *MNRAS*, 460, 1970
- Breger, M. 2000, *Delta Scuti and Related Stars ASP Conf Series in ASPC*, 210, 3
- Breger, M., & Montgomery, M. 2000, *Delta Scuti and Related Stars in ASPC*, 210
- Breger, M., Balona, L., Lenz, P., et al. 2011, *MNRAS*, 414, 1721
- Breger, M., Pamyatnykh, A. A., Pikall, H., & Garrido, R. 1999, *A&A*, 341, 151
- Brown, T. M., Latham, D. W., Everett, M. E., et al. 2011, *AJ*, 142, 112
- Cox, A. N. 2000, *Allen's astrophysical quantities*, 4th ed. Publisher: New York: AIP Press; Springer, ed. Arthur N. Cox
- Cui, X.-Q., Zhao, Y.-H., Chu, Y.-Q., et al. 2012, *RAA (Research in Astronomy and Astrophysics)*, 12, 1197
- Dal, H. A. & Sipahi, E. 2013, *PASA*, 30, e016
- El-Badry, K., Rix, H.-W., Ting, Y.-S., et al. 2018, *MNRAS*, 473, 5043
- Faigler, S., & Mazeh, T. 2011, *MNRAS*, 415, 3921
- Faigler, S., Mazeh, T., Quinn, S.N., Latham, D. W., & Tal-Or, L. 2012, *ApJ*, 746, 185
- García Hernández, A., Moya, A., Michel, E., et al. 2009, *A&A*, 506, 79
- García Hernández, A., Moya, A., Michel, E., et al. 2013, *A&A*, 559, A63
- García Hernández, A., Martín-Ruiz, S., Monteiro, M. J. P. F. G., et al. 2015, *ApJL*, 811, L29
- García Hernández, A., Suárez, J. C., Moya, A., et al. 2017, *MNRAS*, 471, L140
- Gilliland, R. L., Brown, T. M., Christensen-Dalsgaard, J., et al. 2010, *PASP*, 122, 131
- Greiss, S., Steeghs, D., Gänsicke, B. T., et al. 2012, *AJ*, 144, 24
- Hambleton, K. M., Kurtz, D. W., Prša, A., et al. 2013, *MNRAS*, 434, 925
- Hilditch, R. W. 2001, *An Introduction to Close Binary Stars*, 392, (UK: Cambridge University Press)
- Ibanoğlu, C., Soydugan, F., Soydugan, E., et al. 2006, *MNRAS*, 373, 435
- Kahraman Aliçavuş, F., Soydugan, E., Smalley, B., & Kubát, J. 2017, *MNRAS*, 470, 915
- Kallinger, T., Reegen, P., & Weiss, W. W. 2008, *A&A*, 481, 571
- Kjeldsen, H., Christensen-Dalsgaard, J., Handberg, R., et al. 2010, *Astronomische Nachrichten*, 331, 966
- Kjeldsen, H., Bedding, T. R., & Christensen-Dalsgaard, J. 2008, *ApJL*, 683, L175
- Kirk, B., Conroy, K., Prša, A., et al. 2016, *AJ*, 151, 68
- Kreiner, J. M., Kim, C.-H., & Nha, I.-S. 2001, *An Atlas of O-C Diagrams of Eclipsing Binary Stars*, (Poland: Wydawnictwo Naukowe Akademii Pedagogicznej)
- Koch, D. G., et al. 2010, *ApJL*, 713, L79
- Ledoux, P. 1951, *ApJ*, 114, 373
- Lee, J. W., & Park, J.-H. 2018, *MNRAS*, 480, 4693
- Lenz, P., & Breger, M. 2005, *Communications in Asteroseismology*, 146, 53
- Liakos, A. 2015, *Living Together: Planets, Host Stars and Binaries*, 496, 286
- Liakos, A. 2020, *A&A*, 642, A91
- Liakos, A., & Niarchos, P. 2015, *Living Together: Planets, Host Stars and Binaries*, 496, 195
- Liakos, A., & Niarchos, P. 2016, *arXiv e-prints*, arXiv:1606.08638
- Liakos, A., & Niarchos, P. 2017, *MNRAS*, 465, 1181
- Liakos, A., Niarchos, P., Soydugan, E., & Zsche, P. 2012, *MNRAS*, 422, 1250
- Lucy, L. B. 1967, *ZAp*, 65, 89
- Matijević, G., Prša, A., Orosz, J. A., et al. 2012, *AJ*, 143, 123

- Mkrtichian, D. E., Kusakin, A. V., Rodriguez, E., et al. 2004, *A&A*, 419, 1015
- Morris, S. L. 1985, *ApJ*, 295, 143
- Morris, S. L., & Naftilan, S. A. 1993, *ApJ*, 419, 344
- Murphy, S. J., Moe, M., Kurtz, D. W., et al. 2018, *MNRAS*, 474, 4322
- Panchal, A., & Joshi, Y. C. 2021, *AJ*, 161, 221
- Paparó, M., Kolláth, Z., Shobbrook, R. R., et al. 2018, *MNRAS*, 477, 4362
- Prša, A., Batalha, N., Slawson, R. W., et al. 2011, *AJ*, 141, 83
- Rodríguez, E., & Breger, M. 2001, *A&A*, 366, 178
- Ruciński, S. M. 1969, *Acta Astronomica*, 19, 245
- Saio, H. 1981, *ApJ*, 244, 299
- Saio, H., Kurtz, D. W., Takata, M., et al. 2015, *MNRAS*, 447, 3264
- Samadi-Ghadim, A., Lampens, P., Jassur, D. M., et al. 2020, *A&A*, 638, A57
- Skrutskie, M. F., Cutri, R. M., Stiening, R., et al. 2006, *AJ*, 131, 1163
- Slawson, R. W., Prša, A., Welsh, W. F., et al. 2011, *AJ*, 142, 160
- Sterken, C. 2005, *The Light-Time Effect in Astrophysics: Causes and Cures of the O-C Diagram*, 335, 3
- Streamer, M., Ireland, M. J., Murphy, S. J., & Bento, J. 2018, *MNRAS*, 480, 1372
- Suárez, J. C., García Hernández, A., Moya, A., et al. 2014, *A&A*, 563, A7
- Torres, G., Andersen, J., & Giménez, A. 2010, *A&A Rev.*, 18, 67
- Turner, G., & Holaday, J. 2015, *Journal of the American Association of Variable Star Observers (JAAVSO)*, 43, 40
- Uytterhoeven, K., Moya, A., Grigahcène, A., et al. 2011, *A&A*, 534, A125
- van Hamme, W. 1993, *AJ*, 106, 2096
- Welsh, W. F., Orosz, J. A., Aerts, C., et al. 2011, *ApJS*, 197, 4
- Wilson, R. E. 1979, *ApJ*, 234, 1054
- Wilson, R. E. 2012, *AJ*, 144, 73
- Wilson, R. E., & Devinney, E. J. 1971, *ApJ*, 166, 605
- Yang, T., Esamdin, A., Song, F., et al. 2018, *ApJ*, 863, 195
- Yang, T.-Z., & Esamdin, A. 2019, *ApJ*, 879, 59